
Article:
Gilbert, AD, Mason, J and Tobias, SM (2016) Flux expulsion with dynamics. Journal of Fluid Mechanics, 791. pp. 568-588. ISSN 0022-1120

https://doi.org/10.1017/jfm.2016.60

Flux expulsion with dynamics

Journal:	*Journal of Fluid Mechanics*
Manuscript ID	JFM-15-S-1046.R1
mss type:	Standard
Date Submitted by the Author:	n/a
Complete List of Authors:	Gilbert, Andrew; University of Exeter, Mathematics Research Institute Mason, Joanne; University of Exeter, Mathematics Tobias, Steven; University of Leeds, Applied Mathematics
Keyword:	MHD and Electrohydrodynamics, Turbulent Flows, Vortex Flows

Flux expulsion with dynamics

Andrew D. Gilbert[1], Joanne Mason[1] and Steven M. Tobias[2]

[1]Department of Mathematics and Computer Science, College of Engineering, Mathematics and Physical Sciences, University of Exeter, EX4 4QF, UK

[2]Department of Applied Mathematics, University of Leeds, LS2 9JT, UK

(Received xx; revised xx; accepted xx)

In the process of flux expulsion, a magnetic field is expelled from a region of closed streamlines on a $TR_m^{1/3}$ time scale, for magnetic Reynolds number $R_m \gg 1$ (T being the turnover time of the flow). This classic result applies in the kinematic regime where the flow field is specified independently of the magnetic field. A weak magnetic 'core' is left at the centre of a closed region of streamlines, and this decays exponentially on the $TR_m^{1/2}$ time scale.

The present paper extends these results to the dynamical regime, where there is competition between the process of flux expulsion and the Lorentz force, which suppresses the differential rotation. This competition is studied using a quasi-linear model in which the flow is constrained to be axisymmetric. The magnetic Prandtl number R_m/R_e is taken to be small, R_m large, and a range of initial field strengths b_0 is considered.

Two scaling laws are proposed and confirmed numerically. For initial magnetic fields below the threshold $b_{\rm core} = O(UR_m^{-1/3})$, flux expulsion operates despite the Lorentz force, cutting through field lines to result in the formation of a central core of magnetic field. Here U is a velocity scale of the flow and magnetic fields are measured in Alfvén units. For larger initial fields the Lorentz force is dominant and the flow creates Alfvén waves that propagate away. The second threshold is $b_{\rm dynam} = O(UR_m^{-3/4})$, below which the field follows the kinematic evolution and decays rapidly. Between these two thresholds the magnetic field is strong enough to suppress differential rotation leaving a magnetically controlled core spinning in solid body motion, which then decays slowly on a time scale of order TR_m.

1. Introduction

Throughout the universe electrically conducting fluid flows interact with magnetic fields. By the stretching and folding of magnetic field lines, initially weak fields can grow, a process known as dynamo action (Moffatt 1978). As the magnetic field increases in strength it then resists deformation through Lorentz forces exerted on the flow. Eventually a state of fully developed MHD turbulence ensues, composed of a superposition of coherent structures and random eddies interacting with magnetic fields.

In order to understand the complex interactions of flows and magnetic fields over a wide range of spatial and temporal scales it is valuable to investigate simplified models. In geophysical and astrophysical flows, coherent structures are believed to play a key role in generating large scale magnetic fields (Tobias & Cattaneo 2008). Since these structures have correlation times much greater than the turnover time of the turbulence, one of the most illuminating models of flow–field interaction is the effect of a steady fluid flow with closed streamlines — a single closed eddy — on an initially uniform magnetic field.

Motivation for this approach comes from the study of the coupling of magnetic fields and convection (Weiss & Proctor 2014); furthermore in rapidly rotating convection the dynamics may be dominated by long-lived coherent structures taking the form of vortices (Julien *et al.* 2012). The problem has been addressed in a kinematic regime in which the magnetic field is presumed to be so weak as not to affect the flow, which may then be specified and ceases to have any dynamical attributes. This classic problem was first studied for a smooth flow in the pioneering numerical study of Weiss (1966), and by Parker (1966) for the case of a piecewise smooth flow. These works led to identification of the fundamental process of flux expulsion, whereby the field is destroyed within regions of closed streamlines; in cellular flows the resulting magnetic fluxes are then concentrated on bounding separatrices.

The mathematical theory of flux expulsion is elucidated for linear and axisymmetric, smooth flow fields by Moffatt & Kamkar (1983) and for more general streamline geometry by Rhines & Young (1983). The effect of a closed eddy on a weak imposed field at high magnetic Reynolds number R_m (that is, UL/η where U is the characteristic flow speed, L is a characteristic length and η is the magnetic diffusivity) is to expel field towards the cell boundaries on a time scale of order $TR_m^{1/3}$, where $T = L/U$ is the turnover time scale. The key mechanism is the effect of shear or differential rotation in reducing length scales and so accelerating diffusion, be it of magnetic vector potential, passive scalar or vorticity: the useful and general term *shear–diffuse mechanism* was coined by Bernoff & Lingevitch (1994). These studies are elaborated in Bajer (1998) and Bajer, Bassom & Gilbert (2001), referred to as BBG in what follows. In BBG a further time scale is identified at the eddy centre: here any differential rotation must vanish for a smooth flow, and the shear–diffuse process is weaker. The flux expulsion time scale here increases to order $TR_m^{1/2}$ and a weak remnant, which we will call a *magnetic core*, is created and decays exponentially on this time scale.

Our goal in the present paper is to extend these kinematic studies into the dynamical regime, in which the field affects the flow via the Lorentz force. While it is clear that for sufficiently weak magnetic fields kinematic results are recovered, we address the question of the threshold for the field to have a dynamical effect for the classic problem of flux expulsion in an axisymmetric flow. From another viewpoint, the question becomes: for what field strengths (in a two-dimensional flow) will a magnetic field have an impact on the material conservation of vorticity? Many interesting dynamical effects in quasi two-dimensional hydrodynamics in rotating systems, such as zonal flow generation, have been ascribed to the material conservation properties of potential vorticity (Dritschel & McIntyre 2008). It is therefore critical for MHD studies to determine the effect of magnetic fields in modifying these conservation properties. It is known that such dynamical effects of the magnetic field can be subtle, and depend sensitively on molecular values of the transport coefficients. Perhaps the key study that highlights this is Cattaneo & Vainshtein (1991): the authors consider transport in turbulent two-dimensional fluid flows with a mean magnetic field b_0 across the system. For field strengths b_0 (in Alfvén or velocity units) of order $UR_m^{-1/2}$, the mean field becomes dynamically important in suppressing the stretching of Lagrangian parcels and so of transport; see also Vainshtein & Cattaneo (1992), Cattaneo (1994) and more recently Kim (2006), Keating & Diamond (2008) and Keating, Silvers & Diamond (2008). The reason is that the stretching of field leading to small scales (transverse to field lines) is accompanied by increasing magnetic energy, which is only limited by the effect of molecular (not turbulent or effective) diffusion. To put this more bluntly in the magnetic context a 'cascade' (turbulent or otherwise) of field to small scales is far less passive than appears to be the case for

energy or enstrophy in three- or two-dimensional turbulence. Similar effects arise in magnetoconvection (Galloway, Proctor & Weiss 1978; Weiss & Proctor 2014), in which flux expulsion drives magnetic flux to the boundary of convective cells. In dynamical regimes, the resulting peak fields are limited not by equipartition values $b_0 = O(U)$ but can be substantially larger, with dependence on the magnetic diffusivity and fluid viscosity.

To address the problem of dynamical effects and thresholds for flux expulsion, in this paper we will work in the most straightforward setting of a flow with initially circular streamlines permeated by a uniform magnetic field of strength b_0. The problem is set up in section 2, parameterised by b_0 and values of the magnetic Reynolds number R_m and (fluid) Reynolds number R_e. We will work in the quasi-linear approximation in which we keep the fluid flow axisymmetric and truncate the Lorentz force feedback by retaining only the mean azimuthal component. This is reasonable as we are examining the onset of the importance of the Lorentz force in the dynamics. The approach can be justified in some contexts such as dynamos in high Reynolds number rotating flow (as we have here)† (Bassom & Gilbert 1997) and transport and jet formation in geophysical systems, for example see Tobias, Dagon & Marston (2011) and Srinivasan & Young (2012).

In section 3 of the paper we present numerical simulations of the evolution of field and flow (within the quasi-linear model) for a range of initial magnetic field strengths. Here we observe the key competition or race between the processes of flux expulsion and Lorentz force feedback: will the Lorentz force act early enough to halt the stretching in the flow and so defuse the dramatic effect of flux expulsion in destroying the field? Or, will flux expulsion act first and cut elastic field lines so as to remove the Lorentz force feedback and leave a magnetic core behind? We work in a regime in which $R_e \gg R_m \gg 1$ to highlight the transition between these effects without consideration of viscosity, and this gives us our first threshold $b_{\rm core}(\eta)$ for b_0, as discuss below. However we also obtain a second, lower threshold $b_{\rm dynam}(\eta)$, below which the magnetic field has no discernible effect and the kinematic picture holds. In sections 4 and 5 we develop the theory for the two thresholds identified in section 3, based both on the classic asymptotics in Moffatt & Kamkar (1983) and Rhines & Young (1983), and on the more elaborate picture in BBG, which we need to identify the lower threshold. Finally section 6 offers some concluding comments and avenues for further research.

2. Governing equations

Our starting point is the equations for MHD, written in the form

$$\partial_t \boldsymbol{u} + \boldsymbol{u}\cdot\nabla\boldsymbol{u} = \boldsymbol{b}\cdot\nabla\boldsymbol{b} - \nabla p + \nu\nabla^2\boldsymbol{u}, \tag{2.1}$$

$$\partial_t \boldsymbol{b} + \boldsymbol{u}\cdot\nabla\boldsymbol{b} = \boldsymbol{b}\cdot\nabla\boldsymbol{u} + \eta\nabla^2\boldsymbol{b}, \tag{2.2}$$

$$\nabla\cdot\boldsymbol{u} = \nabla\cdot\boldsymbol{b} = 0. \tag{2.3}$$

The two-dimensional flow and field (measured in velocity units) are confined to the plane $z = 0$ in cylindrical polar coordinates (r, θ, z), and setting $\boldsymbol{u} = \nabla\times(\psi\hat{\boldsymbol{z}})$, $\boldsymbol{b} = \nabla\times(a\hat{\boldsymbol{z}})$ we obtain the equations in terms of the stream function ψ, vorticity ω, flux function a,

† Note that in a rotating fluid flow, the axisymmetric component of the Lorentz force can only be balanced against viscous terms, whereas a non-axisymmetric component can be balanced against weak inflows and outflows (cf. the Taylor (1963) constraint), and for this reason the response to the axisymmetric component dominates at large Reynolds number, as in the quasi-linear model.

and current j, all functions of (r,θ,t), as

$$\partial_t\omega = J(\psi,\omega) - J(a,j) + \nu\nabla^2\omega, \tag{2.4}$$

$$\partial_t a = J(\psi,a) + \eta\nabla^2 a, \tag{2.5}$$

$$\omega = -\nabla^2\psi, \quad j = -\nabla^2 a. \tag{2.6}$$

Here the Jacobian is given by $J(\psi,\omega) = r^{-1}[(\partial_r\psi)(\partial_\theta\omega) - (\partial_\theta\psi)(\partial_r\omega)]$.

Following the discussion in Moffatt & Kamkar (1983), we commence with an initial uniform magnetic field in the x-direction and an axisymmetric flow field. Thus ψ and ω are taken to be independent of θ and the fields a and j are represented using an $e^{im\theta}$ dependence with $m = 1$. Although our focus is always on $m = 1$, it is helpful in the analytical development to leave a general, integer value of $m > 0$. We therefore set for the flow

$$\omega = \omega(r,t) + \cdots, \quad \psi = \psi(r,t) + \cdots, \tag{2.7}$$

and for the field

$$a = \tilde{a}(r,t)e^{im\theta} + \text{c.c.} + \cdots, \quad j = \tilde{j}(r,t)e^{im\theta} + \text{c.c.} + \cdots, \quad \boldsymbol{b} = \tilde{\boldsymbol{b}}(r,t)e^{im\theta} + \text{c.c.} + \cdots. \tag{2.8}$$

The tildes denote the harmonic $m > 0$ in θ, but for readability we drop these in what follows.

Now the Lorentz force feedback from the field to the flow will incorporate a mean part, independent of θ, and harmonics $e^{2im\theta}$, which will then proliferate, giving the trailing terms not written down explicitly in (2.7, 2.8). We employ a truncation by neglecting these higher order harmonics, and retain only the terms shown. This leaves the quasi-linear system for the field harmonic m and the mean flow, written compactly as

$$\partial_t a + im\alpha\, a = \eta\Delta_m a, \tag{2.9}$$

$$\partial_t\omega = r^{-1}\partial_r G + \nu\Delta_0\omega. \tag{2.10}$$

The angular velocity is $\alpha(r,t) = -r^{-1}\partial_r\psi$, and the current and vorticity are linked by

$$j = -\Delta_m a, \quad \omega = -\Delta_0\psi, \tag{2.11}$$

where $\Delta_m = \partial_r^2 + r^{-1}\partial_r - m^2r^{-2}$. The Lorentz force term in (2.10) is $G(r,t)$ given by

$$G = im(aj^* - a^*j). \tag{2.12}$$

We will use this quasi-linear approximation to gain an understanding of the essential processes in the competition between flux expulsion and the Lorentz force, both numerically and analytically.

For initial conditions, our focus is on the case of a uniform field in the x-direction of strength b_0, which has current $j = 0$. However we generalise to an arbitary value of m, and consider an initial multipole, current-free field given by the vector potential

$$a(r,0) = -\tfrac{1}{2}ib_0r^m \tag{2.13}$$

(with b_0 real). We also need an initial axisymmetric fluid flow $\boldsymbol{u}$ and have chosen a Gaussian vortex with

$$\omega(r,0) = T^{-1}(4\pi)^{-1}e^{-r^2/4L^2}, \quad \alpha(r,0) = T^{-1}(2\pi r^2/L^2)^{-1}(1-e^{-r^2/4L^2}). \tag{2.14}$$

where L is a length scale, T a time scale, and below $U = L/T$. We will non-dimensionalise the system using these scales and defining, for example:

$$r = L\hat{r}, \quad t = T\hat{t}, \quad \boldsymbol{u} = U\hat{\boldsymbol{u}}, \quad \boldsymbol{b} = U\hat{\boldsymbol{b}}, \quad \nu = UL\hat{\nu}, \quad \eta = UL\hat{\eta}, \tag{2.15}$$

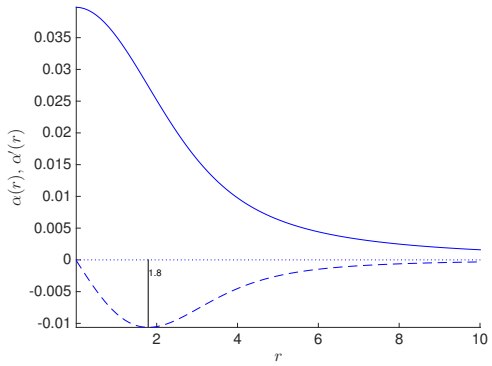

FIGURE 1. The angular velocity profile α (solid) in (2.16) and α' (dashed), with the location of maximal differential rotation $|\alpha'|$ identified as $r^\dagger \simeq 1.8$.

with hats denoting non-dimensional quantities. With this we can also identify $R_m \equiv \hat{\eta}^{-1}$ as a magnetic Reynolds number, $R_e \equiv \hat{\nu}^{-1}$ as a Reynolds number and $M \equiv b_0^{-1}$ as a magnetic Mach number. We will in what follows drop the hats and work with dimensionless quantities, except when we refer to our results in the final discussion section.

Our goal then is to solve the PDEs specified in (2.9–2.12), for the initial conditions (2.13) and now

$$\omega(r,0) = (4\pi)^{-1} e^{-r^2/4}, \quad \alpha(r,0) = (2\pi r^2)^{-1}(1 - e^{-r^2/4}). \tag{2.16}$$

The angular velocity α and differential rotation $\alpha' \equiv \partial_r \alpha$ are depicted in figure 1, where for convenience we often use a prime to denote a radial derivative. The radius $r^\dagger$ marks the location of maximal differential rotation $|\alpha'|$, where we will see that flux expulsion commences in a kinematic regime.

The parameter set comprises the three non-dimensional quantities $\{\eta, \nu, b_0\}$, and we use this form as it is more convenient to place "η" rather than the bulky term "R_m^{-1}" in our calculations. We are interested in the regimes that are realised depending on the strength of the initial field for different diffusive parameters. In this study our primary interest is in the interaction of flux expulsion (depending on η) and the Lorentz force (linked to b_0), rather than viscous effects. We will thus take $\nu \ll \eta$ and so work at a low value of the magnetic Prandtl number $P_m \equiv R_m/R_e = \nu/\eta$.† In all the simulations shown, we have simply taken $P_m = 0.01$, and tests confirm that our results are insensitive to this precise value. Our parameter set is thus reduced to $\{\eta, b_0\}$ and we are interested in thresholds for different types of behaviour, giving b_0 as a function of η with a power law scaling: how strong must the initial field be for the Lorentz force to modify the classic picture of flux expulsion?

Theory for these thresholds is developed in section 4. Before giving numerical results in the next section though, it is worth outlining the origin of the classic approximation for kinematic flux expulsion (for more detail see Moffatt & Kamkar (1983), Rhines & Young (1983)). Consider when there is no dissipation, then the vector potential and current are

† Note that viscous damping would emerge on a time scale of order R_e whereas the effects we consider occur on time scales of order $R_m^{1/3}$ and $R_m^{1/2}$, and thus our results are likely to be correct over a wider range of values of P_m including $P_m = O(1)$.

given by

$$a = -\tfrac{1}{2} i b_0 r^m \, e^{-im\alpha t}, \quad j \simeq -\tfrac{1}{2} i b_0 r^m m^2 \alpha'^2 t^2 \, e^{-im\alpha t}, \tag{2.17}$$

where we have retained in j just the terms that grow fastest, that is quadratically with time t. For small η, then, the right-hand side $\eta \Delta_m a = -\eta j$ in (2.9) grows quadratically from small values and the accumulated effect of the dissipation gives a term cubic in t. Incorporating this damping in the evolution of a then yields the approximate solution

$$a \simeq -\tfrac{1}{2} i b_0 r^m \, e^{-im\alpha t - \frac{1}{3}\eta m^2 \alpha'^2 t^3}, \quad j \simeq -\tfrac{1}{2} i b_0 r^m m^2 \alpha'^2 t^2 \, e^{-im\alpha t - \frac{1}{3} m^2 \eta \alpha'^2 t^3}. \tag{2.18}$$

This gives dramatic suppression of the vector potential and so of the magnetic field, which commences at the radius $r^\dagger$ where $|\alpha'|$ is maximised, indicated on figure 1 for the Gaussian profile (2.16), on a timescale $t^\dagger = O(\eta^{-1/3})$.† Specifically $r^\dagger$ and $t^\dagger$ (up to an order one constant) are given by

$$r^\dagger = \arg\max_r |\alpha'(r)|^2, \quad t^\dagger = [\tfrac{1}{3} m^2 \eta \alpha'(r^\dagger)^2]^{-1/3}. \tag{2.19}$$

The dagger helpfully denotes the cutting of magnetic field lines caused by flux expulsion.

For our purposes there are two problems with this approximation. The first is that the Lorentz force term (2.12) vanishes identically to this order. The next order terms need to be taken into account, and we undertake this in a systematic development in section 4.2. The second issue is discussed in BBG and is that this approximation breaks down near the origin where $\alpha' \to 0$. In other words the approximation is predicated on a shear $\alpha' = O(1)$ that makes the quadratic multiplier t^2 in j in (2.18) dominant; towards the centre of a vortex another, inner approximation has to be used. Although this may seem a technical issue, in fact it is key to understanding the dynamical problem, and we develop this in section 4.1 following BBG. In preparation for this we note here that the angular velocity in (2.16) behaves as $r \to 0$ according to

$$\alpha = \alpha_0 + \alpha_1 r^2 + \alpha_2 r^4 + \cdots, \tag{2.20}$$

$$\alpha_0 = 1/8\pi, \quad \alpha_1 = -1/64\pi. \tag{2.21}$$

From the point of view of the kinematic problem, with the axisymmetric flow specified independent of the field, the form (2.20) gives the behaviour near the origin. Smoothness considerations eliminate any odd powers of r and generically the constant α_1 is non-zero. This constant plays an important role in kinematic theory as it controls how the differential rotation α' responsible for flux expulsion switches off near the origin. Dynamically the magnetic field can change the form of the flow near the origin, as we shall see. We also note that the numerical values of α_0 and particularly $\alpha_1 \simeq -1/200$ are rather low, meaning that the turnover time of the flow is large in our non-dimensionalisation and making the corresponding time scales appear long on our plots. For best comparison with simulations we will retain factors of α_1 in our theoretical development.

3. Numerical simulations

3.1. *Illustrative runs*

Our goal in this section is to present numerical simulations of the model (2.9–2.12) with the initial conditions (2.13, 2.16). This will motivate the theory in the next section, but we will also refer ahead to results in that section. Our parameters are only $\{\eta, b_0\}$

† Naturally, in the kinematic problem this profile is taken to be fixed for all t and not viscously damped; only the magnetic field evolves via (2.9) in the given flow field with $\alpha(r,t) = \alpha(r,0)$.

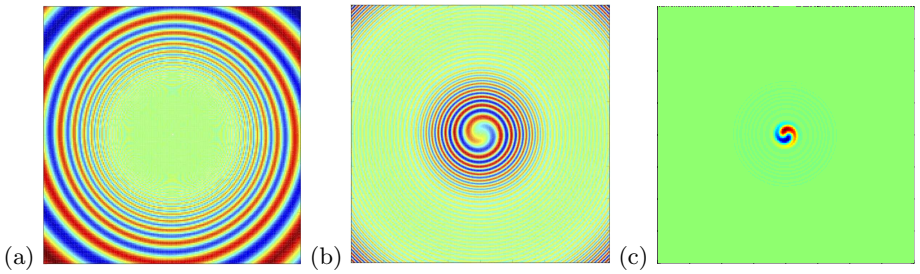

(a) (b) (c)

FIGURE 2. Kinematic magnetic field evolution. In (a,b) $t = 10^4$ and (c) 4×10^4. In (a) $-10 \leqslant x, y \leqslant 10$, while in (b,c) only the central region $-2 \leqslant x, y \leqslant 2$ is depicted.

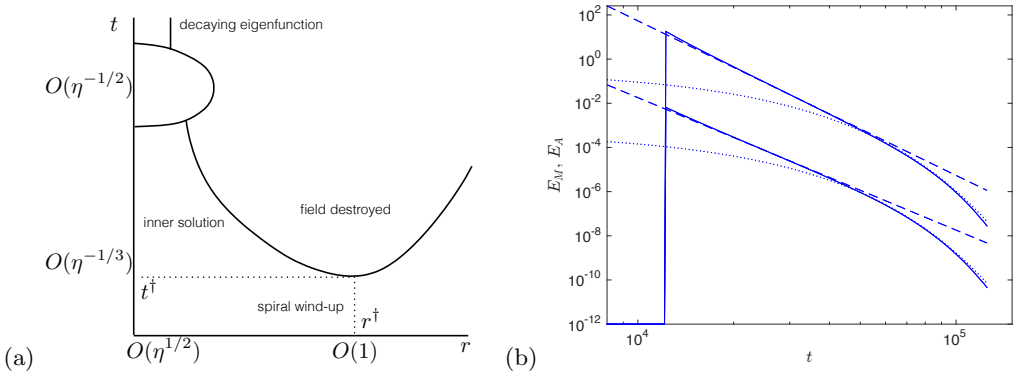

(a) (b)

FIGURE 3. (a) Schematic of kinematic evolution of magnetic field for $\eta \ll 1$, and (b) log–log plot of E_M (upper solid) and E_A (lower solid) as functions of time t. In (b) the scaling laws t^{-7} (4.10) and t^{-6} (4.11) are depicted (dashed), and the formulae (4.13), (4.14) are shown (dotted).

and we first show the various phenomena that occur when we fix $\eta = 10^{-7}$ (with $m = 1$, $\nu = 0.01\eta$ as always), and allow a range of values of b_0.

Our starting point is the kinematic problem when the field b_0 is sufficiently weak that dynamical effects may be neglected. Although the Lorentz force feedback is easily switched off in our simulations, one of our goals is to quantify just how weak the initial field b_0 needs to be for kinematic theory to apply, for $\eta \ll 1$. In any case we integrate (2.9) in isolation. Figure 2 shows colour scale plots of the vector potential reconstructed from (2.8), so that lines of constant colour give magnetic field lines, from blue (low values of a in (2.8)) to red (high values); zero or weak a is green. The panels show different times, and in each panel the colour scale is normalised separately on the maximum/minimum vector potential for that panel. Panel (a) gives a wide view, showing spiral wind-up of field lines by the flow and suppression of magnetic field by diffusion for moderate r. Panels (b,c) show a zoom into the central region, where the onset of flux expulsion around $r^\dagger$ can be seen in (b), followed by further destruction of field leading to the final phase in (c), of a decaying, remnant field structure localised at the origin.

Figure 3 shows a schematic of kinematic field evolution (adapted from BBG): at $t^\dagger = O(\eta^{-1/3})$ there is the onset of flux expulsion at a radius $r^\dagger$. This then spreads outwards and inwards, as indicated in (2.18). At late times $t = O(\mathcal{T}) = O(\eta^{-1/2})$ (see (4.1)) this wave of destruction reaches the centre of the axisymmetric flow and all that is left behind is a rotating, exponentially decaying remnant, an eigenfunction of the scalar advection equation, seen in figure 2(c).

For times greater than the flux expulsion onset time $t^\dagger$, we can identify the field inside $r^\dagger$ as the magnetic *core* and it is convenient to define the corresponding magnetic energy

(a) 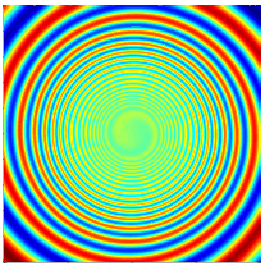 (b) 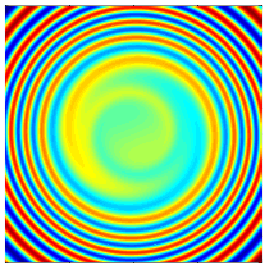 (c) 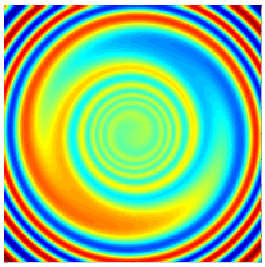

FIGURE 4. Magnetic field evolution for $b_0 = 5 \times 10^{-4}$. The region $-10 \leqslant x, y \leqslant 10$ is shown for (a) 10^4, (b) 2×10^4 and (c) 2.5×10^4.

(a) 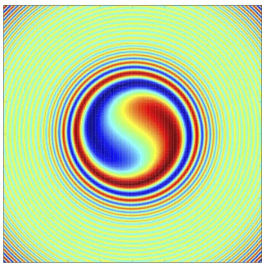 (b) 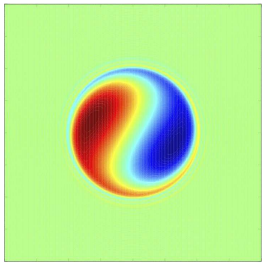 (c) 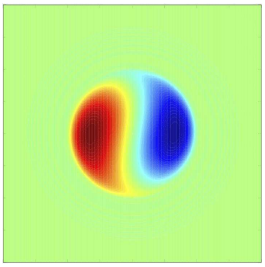

FIGURE 5. Magnetic field evolution for $b_0 = 2 \times 10^{-4}$. The central region $-2 \leqslant x, y \leqslant 2$ is shown for (a) $t = 10^4$, (b) 2×10^4 and (c) 5×10^4.

and (half) the integrated square vector potential by

$$E_M(t) = \int_0^{r^\dagger} 2\pi r\, |\boldsymbol{b}|^2\, dr, \quad E_A(t) = \int_0^{r^\dagger} 2\pi r\, |a|^2\, dr. \tag{3.1}$$

These are shown as functions of time in the log–log plot figure 3(b): commencing at $t^\dagger \simeq 1.2 \times 10^4$ they rapidly adopt a t^{-7} (4.10) and t^{-6} (4.11) decay in time. At time of order $\mathcal{T} \simeq 3.2 \times 10^4$ (4.1) the power law decay is replaced by exponential decay (4.13), (4.14). Note that there is no absolute definition of $t^\dagger$: instead for practical purposes we check when $|a(r,t)| < \delta |a(0,t)|$ with a small number δ: the earliest time at which this occurs determines $t^\dagger$, with $r^\dagger$ as the corresponding radius. We have chosen $\delta = 0.001$ for results shown here: other values make minor changes to the values of $t^\dagger$ but do not affect $r^\dagger \simeq 1.8$ and make no visible difference to the curves for E_M or E_A once a magnetic core is so defined.

We now leave the kinematic problem and report on runs for varying values of the initial magnetic field b_0. First figure 4 shows a run for a relatively strong field $b_0 = 5 \times 10^{-4}$. Here we see the process of spiral wind-up commence in (a), but stretching of magnetic field lines saps energy from the flow field, reducing the shear and stopping the flux expulsion process. In panels (b,c) we see the field in the simulation start to unwind, reversing the direction of the original vortex. This disturbance then propagates outwards to hit the numerical boundary and, unphysically, bounces back and forth (not shown). In reality the original flow would turn into Alfvén waves propagating to infinity along the field lines. For this reason we do not spend further effort on the cases where the field is *above* the threshold for flux expulsion to occur, even though one of our primary goals is to establish this threshold, working from below.

We now reduce the initial field b_0 in subsequent plots, starting with figure 5 which shows magnetic field evolution for $b_0 = 2 \times 10^{-4}$. In this case flux expulsion occurs to cut the field lines at around $r^\dagger \simeq 1.8$; see panel (a). However once the field lines are

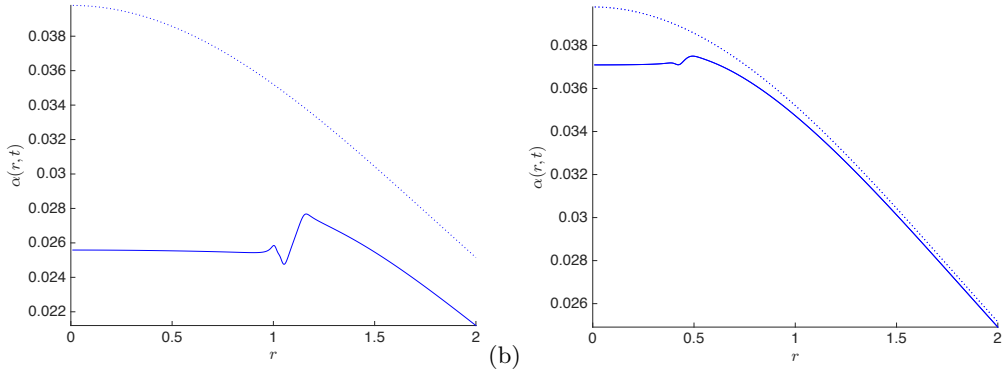

FIGURE 6. Final angular velocity profiles for (a) $b_0 = 2 \times 10^{-4}$ in figure 5 and (b) 5×10^{-5} in figure 7, for $t = 5 \times 10^4$. The function $\alpha(r, t)$ (solid) is plotted against r, with the initial profile $\alpha(r, 0)$ shown dotted.

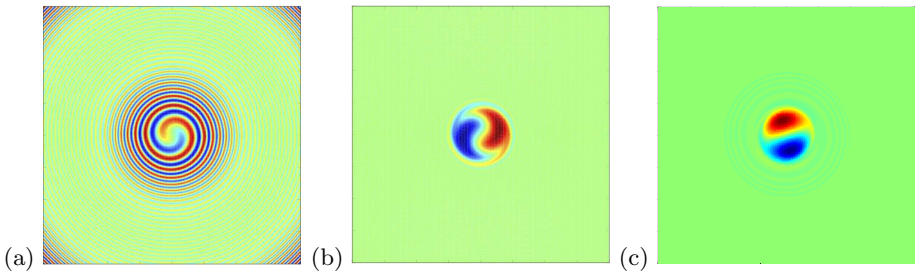

FIGURE 7. Magnetic field evolution for $b_0 = 5 \times 10^{-5}$. The central region $-2 \leqslant x, y \leqslant 2$ is shown for (a) $t = 10^4$, (b) 2×10^4 and (c) $t = 5 \times 10^4$.

cut to leave a magnetic core, the Lorentz force now acts to reduce field line curvature and magnetic energy within the core, in panel (b). What remains is a core consisting of two lobes of field relaxed to a state of low energy, and the flow field is modified so that there is solid body rotation in the region occupied by the field, shown in figure 6(a). We say that a *dynamical core* has been formed, dynamical as the Lorentz force has acted to control the flow. This core will then decay, but on a longer Ohmic time scale (presumably $O(\eta^{-1})$, though we will not try to verify this).

Finally figure 7 shows evolution of a yet weaker field $b_0 = 5 \times 10^{-5}$. Here again there is a process of flux expulsion leaving a core which shrinks as the field is diffusively destroyed. The Lorentz force again acts to leave a flattened region in the flow field, constant angular velocity seen in figure 6(b), and a dynamical core with two lobes, albeit now smaller than in the previous case. For fields yet weaker than this, we soon find results that become indistinguishable from the kinematic regime in figure 2 and no dynamical core forms.

Another viewpoint is given in figure 8 which plots (a) E_M and (b) E_A against time for a range of b_0. In each panel the lowest, dashed curves gives the kinematic time traces (from figure 2). For strong fields (highest, outermost curves), the onset $t^\dagger$ of flux expulsion is delayed and the field decays very slowly, noting that E_M shows oscillations (torsional oscillations) while the dynamical magnetic core relaxes. On the other hand E_A behaves monotonically, as it must since the quantity a obeys a scalar advection–diffusion equation. As the initial field is reduced the traces follow the kinematic curves for a period and then depart: this marks the formation of a dynamically controlled core sitting in a region of solid body motion. Finally very weak field follows the kinematic traces.

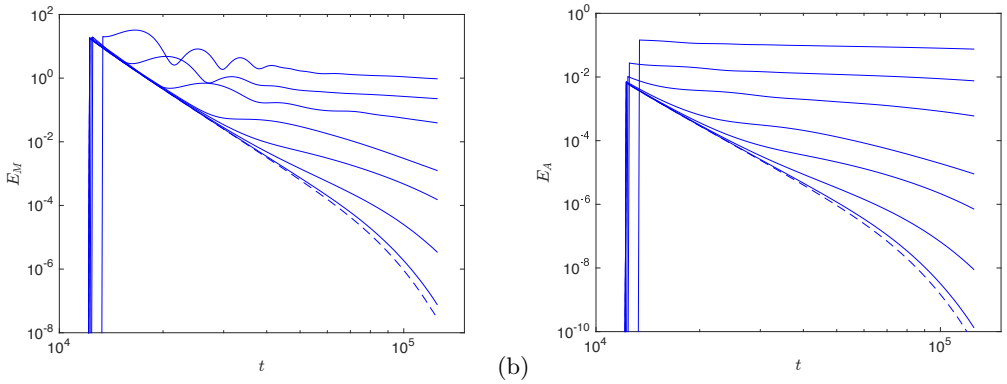

FIGURE 8. Plotted is (a) the magnetic energy E_M and (b) E_A as functions of time t for varying field strength b_0. The dashed curves are kinematic traces, while $b_0 = 2 \times 10^{-4}$, 10^{-4}, 5×10^{-5}, 2×10^{-5}, 10^{-5}, 5×10^{-6} and 2×10^{-6}, going down the curves on the right of the plots.

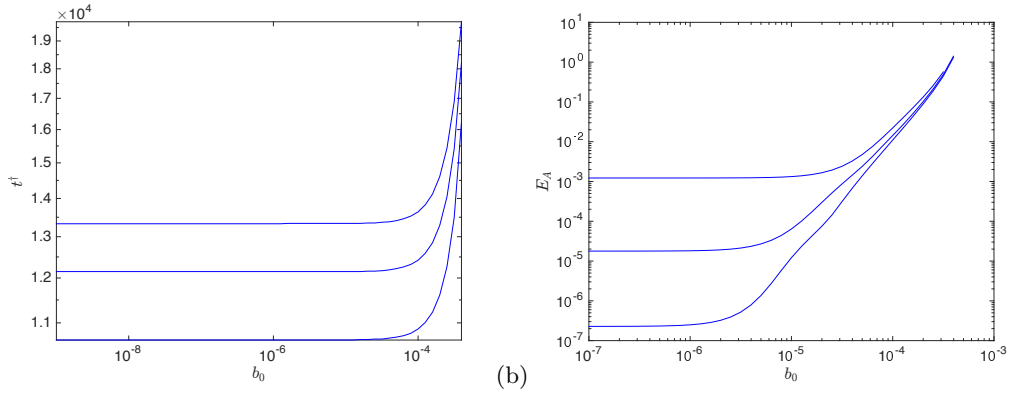

FIGURE 9. (a) The onset of flux expulsion $t^\dagger$ as a function of initial field strength b_0 using different thresholds $\delta = 10^{-4}$, 10^{-3}, and 10^{-2}, reading down the curves. (b) E_A plotted against b_0 at times $\frac{1}{2}\mathcal{T}$, $\mathcal{T}$ and $2\mathcal{T}$, reading down the curves.

3.2. *Thresholds and scaling laws*

We can summarise the results of the previous section as the presence of two thresholds. For a given flow field, the first is the threshold $b_0 = b_{\rm core}(\eta)$ above which the Lorentz force is so strong that flux expulsion does not occur and so $t^\dagger$, E_M and E_A cannot be defined. Figure 9(a) shows $t^\dagger$ as measured numerically using several values of δ (see below (3.1)). There is a sharp transition from the onset of flux expulsion at a time independent of initial field strength, to one that diverges rapidly with b_0; at the same time the radius $r^\dagger$ increases from 1.8 to around 2.2 (not shown). This sharp transition makes the threshold $b_0 = b_{\rm core}(\eta)$ easy to measure, at least approximately.

The second, lower threshold is $b_0 = b_{\rm dynam}(\eta)$ above which the field is sufficiently strong (i.e. sufficiently *dynamical*) to modify the flow field and suppress diffusive decay. In this case the Lorentz force opposes differential rotation and results in solid body motion in a region near the origin. In terms of the flow field, this has the effect of turning off α_1 in (2.20) and so removes the weak differential rotation at the origin that otherwise controls the exponential decay of the core in the kinematic regime; see figure 3(a) and section 4.1. Above the threshold we are left with a slowly decaying dynamical core. To measure this threshold we have considered the quantity E_A; (unlike E_M this is free from torsional

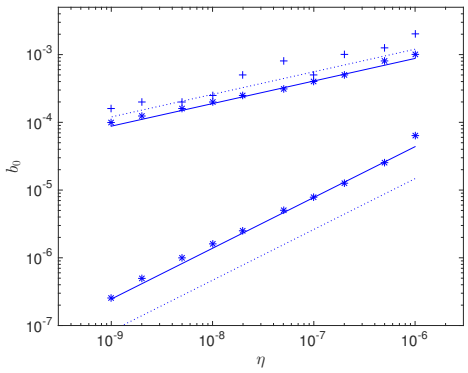

FIGURE 10. Thresholds $b_{\rm core}(\eta)$ (upper dataset) and $b_{\rm dynam}(\eta)$ (lower dataset) plotted against η. In each case the data points come from a series of runs with varying b_0. The solid lines give the scalings $\eta^{1/3}$ (upper) and $\eta^{3/4}$ (lower). The dotted lines give the scalings from (5.4) and (5.7).

oscillations — see figure 8) at three times $\frac{1}{2}\mathcal{T}$, $\mathcal{T}$ and $2\mathcal{T}$ and plot this against b_0 in figure 9(b). Where the curves cluster together on the right-hand side, the energy decays negligibly on the $\mathcal{T}$ time scale and we are in the dynamical core regime. Where the curves are spread out on the left-hand side, the field is so weak that the evolution is kinematic with a core decaying rapidly, that is, on the $\mathcal{T}$ time scale. The somewhat broad transition between these marks the threshold $b_{\rm dynam}(\eta)$, for this value of η.

Neither of these thresholds is precisely defined, but in any case we are primarily interested simply in how they scale with η. We select a representative transitional field strength $b_{\rm dynam}$ to be the initial value of b_0 for which $\log[E_A(2\mathcal{T})/E_A(\mathcal{T})]$ is half of its kinematic value. We estimated $b_{\rm dynam}$ using a series of runs with 10 values of b_0 per decade on the logarithmic scale. For example in figure 9 we obtain $b_{\rm dynam} = 7.9\times10^{-6}$ for $\eta = 10^{-7}$. Figure 10 shows $b_{\rm dynam}$ estimated this way, in the lower dataset, showing good agreement with the scaling law $b_{\rm dynam} \sim \eta^{3/4}$ (solid) from (5.5).

To estimate the threshold $b_{\rm core}(\eta)$ for core formation we adopt two methods and these are shown in the upper dataset in figure 10. The first is obtained by selecting the minimum field strength b_0 for which the ratio $E_A(\mathcal{T})/E_A(2\mathcal{T}) < 1.08$ (asterisks), and this shows a good fit to the scaling law $b_{\rm core} \sim \eta^{1/3}$ in (5.3), with $b_{\rm core} \simeq 4\times10^{-4}$ at $\eta = 10^{-7}$. For another method, we chose the largest b_0 for which core formation, that is the existence of a value of $t^\dagger$, was detected in our code (plus signs), giving $b_{\rm core} \simeq 5\times10^{-4}$ at $\eta = 10^{-7}$. This also confirms the scaling law, albeit with more scatter. Note that alternatively we can use the scalings to rescale the vertical and the horizontal axes in figure 9(a,b) for a set of values of η and so collapse the curves, which works well but which we do not show here.

Finally we comment on the numerical methods used. Equations (2.9–2.12) were written as a system of six first order PDEs for the real and imaginary parts of a, $\partial_r a$, and v, $\partial_r v$. This system was then passed to the NAG solver `d03pef`, which employs a Keller box method and integrates in time, with $r_{\rm lo} \leqslant r \leqslant r_{\rm hi}$ for $r_{\rm lo} = 0.05$, $r_{\rm hi} = 20$ and up to 2×10^4 radial gridpoints in typical runs. At the inner and outer boundaries, the condition of behaviour as r^m was imposed on the vector potential, namely $r\partial_r a - ma = 0$. For the flow component v, the code similarly imposed behaviour proportional to r at the inner boundary, and to r^{-1} at the outer. In the cases where flux expulsion occurs and

a magnetic core is formed, the outer boundary does not play a role, as discussed above, and $r_{\rm hi} = 20$ is sufficiently large (at least over the time scales shown here).

4. Calculation of the Lorentz force feedback

Our goal in this section is to derive the various scaling laws above, in particular those in figure 10. It is evident from figure 8 that the kinematic evolution is key, in that the dynamical curves typically follow the kinematic evolution, at least for a time. We consider the kinematic regime, corresponding to the limit $b_0 \to 0$ and a fixed flow field. We then assess the feedback on the flow through the Lorentz force.

4.1. *Flux expulsion: inner solution*

We begin by recalling the classic flux expulsion calculation yielding (2.18) as an approximate *outer solution* to the equation (2.9). This gives a and j at radii where $\alpha'(r) \neq 0$ (fixed as $\eta \to 0$) and is valid for a general smooth profile $\alpha(r)$. However the approximation breaks down at the centre of the flow field where $\alpha'(0) = 0$ necessarily, and so another approximation, the *inner solution*, is needed there. Generally we assume that $\alpha(r)$ expands as (2.20) with $\alpha_1 \neq 0$,† working in a kinematic regime, but we note that in a dynamical regime the Lorentz force acts to suppress differential rotation given by $\alpha'(r)$. The kinematic theory is provided in BBG and is most easily set out by defining a length scale $\mathcal{L}$, time scale $\mathcal{T}$, their inverses, and a velocity scale $\mathcal{V}$ by

$$k \equiv \mathcal{L}^{-1} = (m\alpha_1/2\eta)^{1/4}, \quad p \equiv \mathcal{T}^{-1} = (2\eta m\alpha_1)^{1/2}, \quad \mathcal{V} = \mathcal{L}/\mathcal{T} = (8\eta^3 m\alpha_1)^{1/4}, \quad (4.1)$$

and new variables by

$$\tau = pt, \quad \rho = kr. \quad (4.2)$$

The exact solution to (2.9) may then be obtained with only the quadratic term retained in $\alpha(r)$ in (2.20), that is $\alpha \simeq \alpha_1 r^2$ (where we also set $\alpha_0 = 0$ as solid body rotation is irrelevant). The solution is

$$a = -\tfrac{1}{2} i b_0 k^{-m} \rho^m g\, e^{-if\rho^2}, \quad (4.3)$$

$$j = -\tfrac{1}{2} i b_0 k^{2-m} \rho^m g\, [4i(m+1)f + 4f^2\rho^2]\, e^{-if\rho^2}, \quad (4.4)$$

where $f(\tau)$ and $g(\tau)$ satisfy

$$\partial_\tau g = -2i(m+1)fg, \quad \partial_\tau f - 1 = -2if^2, \quad (4.5)$$

and so

$$f(\tau) = (1+i)^{-1} \tanh[(1+i)\tau], \quad g(\tau) = \{\cosh[(1+i)\tau]\}^{-m-1}. \quad (4.6)$$

Now once a core has formed, for $t > t^\dagger$, undertaking the integrals in (3.1) gives straightforwardly

$$E_M = \pi(m+1)!\, b_0^2\, k^{-2m} |g|^2 |f|^2\, (-2f_{\rm i})^{-m-2}, \quad (4.7)$$

$$E_A = \tfrac{1}{4}\pi\, m!\, b_0^2\, k^{-2m-2} |g|^2\, (-2f_{\rm i})^{-m-1}, \quad (4.8)$$

with $f = f_{\rm r} + i f_{\rm i}$ for brevity.

This is all exact if $\alpha(r)$ is given by only the leading terms, in α_0 and α_1 in (2.20).

† Note that the theoretical development in section 4 below is written as if α_1 is positive to follow BBG but the final results are dependent only on $|\alpha_1|$ in any case. There are also several inessential notational differences between the theory in the earlier paper and in the self-contained development here.

The solution combines two different processes, with a crossover time $\mathcal{T}$ defined in (4.1). For $t \ll \mathcal{T}$, the approximation captures a wave of flux expulsion, destruction of a, in the locally quadratic angular velocity profile (2.20). In this regime, we have

$$f = \tau - \tfrac{2}{3}i\tau^3 + \cdots, \quad g \simeq 1, \quad -2f_{\rm i} \simeq \tfrac{4}{3}\tau^3, \tag{4.9}$$

giving

$$E_M \simeq \pi(\tfrac{4}{3})^{-m-2}(m+1)!\, b_0^2\, k^{-2m}\, \tau^{-3m-4} = O(t^{-3m-4}), \tag{4.10}$$

$$E_A \simeq \tfrac{1}{4}\pi(\tfrac{4}{3})^{-m-1}\, m!\, b_0^2\, k^{-2m-2}\, \tau^{-3m-3} = O(t^{-3m-3}), \tag{4.11}$$

and so algebraic behaviour of these quantities, with dependence as t^{-7} and t^{-6} in the important case $m = 1$ of an initial uniform field, as seen in figure 4.

On the other hand for $t \gg \mathcal{T}$ the solution describes an exponentially decaying core taking a Gaussian form near the origin, with

$$f \simeq (1+i)^{-1}, \quad g \simeq 2^{m+1}\, e^{-(m+1)(1+i)\tau}, \quad -2f_{\rm i} \simeq 1, \tag{4.12}$$

and

$$E_M \simeq 2^{2m+1}\, \pi\, (m+1)!\, b_0^2\, k^{-2m}\, e^{-2(m+1)\tau}, \tag{4.13}$$

$$E_A \simeq 2^{2m}\, \pi\, m!\, b_0^2\, k^{-2m-2}\, e^{-2(m+1)\tau}. \tag{4.14}$$

Again this is confirmed by the results shown in figure 4 for $m = 1$.

4.2. *Lorentz force from the outer solution*

We need to evaluate the Lorentz torque G in (2.12) from the outer solution; however there is a cancellation at leading order when we substitute a and j from (2.18). To compute G we need to expand the flux expulsion solution systematically. This is most easily done by setting

$$a = -\tfrac{1}{2}ib_0 r^m\, e^{-im\alpha t + \chi}, \tag{4.15}$$

where the complex function χ, of space and time, gives the effect of flux expulsion. The current and Lorentz force are then

$$\begin{aligned} j = -\tfrac{1}{2}ib_0 r^m \{ & m^2\alpha'^2 t^2 + im[\alpha'' + (2m+1)\alpha' r^{-1} + 2\alpha'\chi']t \\ & - [\chi'' + \chi'^2 + (2m+1)\chi' r^{-1}]\}\, e^{-im\alpha t + \chi}, \end{aligned} \tag{4.16}$$

$$\begin{aligned} G = \tfrac{1}{4}mb_0^2 r^{2m} \{ & 2m[\alpha'' + (2m+1)\alpha' r^{-1} + \alpha'(\chi' + \chi'^*)]t \\ & + i[(\chi'' - \chi''^*) + (\chi'^2 - \chi'^{*2}) + (2m+1)\,(\chi' - \chi'^*) r^{-1}]\} e^{\chi + \chi^*}, \end{aligned} \tag{4.17}$$

without approximation.

Now to calculate χ we introduce $T = \eta^{1/3}t$ as the time scale on which flux expulsion occurs, and set $\chi = \chi(r, T)$. The exact equation for χ follows from (2.9) and is

$$\partial_T \chi = -m^2\alpha'^2 T^2 - im\eta^{1/3}[\alpha'' + (2m+1)\alpha' r^{-1} + 2\alpha'\chi']T + \eta^{2/3}[\chi'' + \chi'^2 + (2m+1)\chi' r^{-1}], \tag{4.18}$$

where as usual the prime denotes an r-derivative at constant T (or t). A series approximation for χ can now be developed, with expansion parameter $\eta^{1/3} \ll 1$. Explicitly

$$\chi(r, t) = \chi_0(r, T) + \eta^{1/3}\chi_1(r, T) + \cdots, \tag{4.19}$$

with

$$\chi_0 = -\tfrac{1}{3}m^2\alpha'^2T^3 = -\tfrac{1}{3}m^2\eta\alpha'^2t^3, \tag{4.20}$$

$$\chi_1 = -\tfrac{1}{2}im[\alpha'' + (2m+1)\alpha' r^{-1}]T^2 + \tfrac{4}{15}im^3\alpha'^2\alpha''T^5 \tag{4.21}$$

$$= -\tfrac{1}{2}im[\alpha'' + (2m+1)\alpha' r^{-1}]\eta^{2/3}t^2 + \tfrac{4}{15}im^3\eta^{5/3}\alpha'^2\alpha''t^5. \tag{4.22}$$

To obtain the Lorentz torque at leading order (first line of terms in G in (4.17)) we need only χ_0, which then gives

$$G \simeq \tfrac{1}{2}m^2b_0^2r^{2m}\{[\alpha'' + (2m+1)\alpha' r^{-1}]t - \tfrac{4}{3}m^2\eta\alpha'^2\alpha''t^4\}\, e^{-\frac{2}{3}m^2\eta\alpha'^2t^3}. \tag{4.23}$$

Here we see that despite the initial quadratic growth with time t of the current j in (2.18), the Lorentz torque G grows only linearly via the first two terms (the latter term being small for $t = O(1), \eta \ll 1$). However at the time of flux expulsion $t = O(\eta^{-1/3})$ all the terms in G in (4.23) are of the same order, and so all are important in computing the Lorentz force up to and during the destruction of field through flux expulsion.

4.3. *Feedback through the Lorentz force: outer solution*

We now discuss the effects of the Lorentz force on the flow: this features in the evolution of azimuthal velocity v,

$$\partial_t v = r^{-1}G + \nu(\Delta_0 v - r^{-2}v), \tag{4.24}$$

which in turn gives the equation for the angular velocity gradient α',

$$\partial_t\alpha' = (r^{-2}G)' + \nu[r^{-1}(\Delta_0 v - r^{-2}v)]'. \tag{4.25}$$

It is this key quantity we shall use. Our working hypothesis is that the Lorentz force has the effect of flattening the angular velocity at radius r if the term $(r^{-2}G)'$ evaluated kinematically and integrated over all time, is comparable or bigger than α' at that radius. The threshold to consider is then when

$$\alpha'(r) \sim \int_0^\infty [r^{-2}G(r,t)]'\, dt. \tag{4.26}$$

Bearing in mind that the right hand side is quadratic in b_0 and we are interested in thresholds in terms of b_0, we set the key function we need as

$$h(r) = -\alpha'(r)^{-1}\, b_0^{-2} \int_0^\infty [r^{-2}G(r,t)]'\, dt. \tag{4.27}$$

The minus sign here arises as in (4.25) it is the integral on the right hand side which is being compared with *reducing* the angular velocity gradient from $\alpha'(r)$ at $t = 0$ to zero at large times t. We will take up the discussion of the physics in section 5, but for the moment just focus on calculating $h(r)$ for the outer solution and then the inner one.

First we take G as given from (4.23) with $m = 1$ now (to avoid unnecessary complexity) and obtain

$$[r^{-2}G]' = \tfrac{1}{2}b_0^2[G_0(r)t + G_1(r)\eta t^4 + G_2(r)\eta^2t^7]\, e^{-\frac{2}{3}\eta\alpha'^2t^3}\,, \tag{4.28}$$

with

$$G_0(r) = \alpha''' + 3\alpha''r^{-1} - 3\alpha' r^{-2}, \quad G_1(r) = -4\alpha'\alpha''(\alpha'' + \alpha' r^{-1}) - \tfrac{4}{3}\alpha'^2\alpha''', \quad G_2(r) = \tfrac{16}{9}\alpha'^3\alpha''^2. \tag{4.29}$$

Finally we integrate (4.28) from time zero to infinity using integration by parts and by setting the constant c_0 defined by

$$c_0 = \int_0^\infty t\exp(-t^3)\, dt = 3^{-2/3}\pi\,\mathrm{Hi}'(0) \simeq 0.45137, \tag{4.30}$$

(see Olver *et al.* 2010, section 9.12) to obtain

$$h(r) = -c_1\eta^{-2/3}\alpha'^{-7/3}\,[G_0(r) + \alpha'^{-2}G_1(r) + \tfrac{5}{2}\alpha'^{-4}G_2(r)], \quad c_1 \equiv 2^{-5/3}3^{2/3}c_0, \quad (4.31)$$

or, with the formulae for the $G_j(r)$ in (4.29) we obtain

$$h(r) = c_1\eta^{-2/3}\alpha'^{-7/3}\,[\tfrac{1}{3}\alpha''' + \alpha''r^{-1} + 3\alpha'r^{-2} - \tfrac{4}{9}\alpha''^2\alpha'^{-1}]. \quad (4.32)$$

This (implausible-looking) expression is correct for any $\alpha(r)$. However note that when we approach the origin, $\alpha(r)$ expands as in (2.20) and then

$$h(r) \simeq c_2\eta^{-2/3}\alpha_1^{-4/3}r^{-10/3}, \quad c_2 \equiv 2^2 3^{-4/3}c_0. \quad (4.33)$$

This is valid in the *overlap region* $\mathcal{L} \ll r \ll 1$ where both inner and outer solutions are valid (referring to figure 3). Before using this, we proceed to look at the feedback in the inner solution.

4.4. *Feedback through the Lorentz force: inner solution*

Near the origin where the above formulation breaks down, we need to use the inner solution (4.1–4.6) instead, which yields

$$G = mb_0^2|g|^2k^{2-2m}\rho^{2m}(f+f^*)[(m+1) - i(f-f^*)\rho^2]e^{-i(f-f^*)\rho^2} \quad (4.34)$$

and hence (with $m = 1$) we find

$$(r^{-2}G)' = 2b_0^2|g|^2k^3(f^2 - f^{*2})[-3i\rho - (f-f^*)\rho^3]e^{-i(f-f^*)\rho^2}. \quad (4.35)$$

Now to obtain $h(r)$ in (4.27) we divide by b_0^2 and by $\alpha' = 2\alpha_1 k^{-1}\rho$ and integrate over all time. With the use of (4.1) we obtain

$$h(\rho) = \mathcal{V}^{-2}\int_0^\infty |g|^2(f^2 - f^{*2})[3i + (f-f^*)\rho^2]e^{-i(f-f^*)\rho^2}\,d\tau. \quad (4.36)$$

We have taken the liberty of thinking of h now as a function of $\rho = kr$ and taken the integral over $\tau = pt$. We cannot evaluate this analytically, except for large ρ when the approximation (4.9) is valid throughout the time range giving the leading contribution to the integral, with

$$h(\rho) \simeq c_3\mathcal{V}^{-2}\rho^{-10/3}, \quad c_3 \equiv 2^{8/3}3^{-4/3}c_0. \quad (4.37)$$

This is valid in the overlap region $1 \ll \rho \ll \mathcal{L}^{-1}$ and making use of the definitions of p, k and ρ in (4.1) we recover (4.33) as we must. More generally we can plot $\mathcal{V}^2h(\rho)$ in (4.36) against ρ as in figure 11 to give a universal curve for the Lorentz feedback at the centre of a vortex with a general, smooth angular velocity profile (that is, with $\alpha_1 \neq 0$).

5. Scaling laws and related information

We can use the results in the last section to make a number of predictions for scaling laws. We begin with crude estimates and then give more precise versions. Our aim is to evaluate the accumulated effect of the Lorentz force at a given radius r in a kinematic regime and compare this with $\alpha'(r)$ at that radius. We use $\gtrsim$ and $\lesssim$ to denote inequality up to a constant of order unity. Recall that we are comparing

$$\alpha'(r) \quad \text{and} \quad \int_0^\infty [r^{-2}G(r,t)]'\,dt \quad (5.1)$$

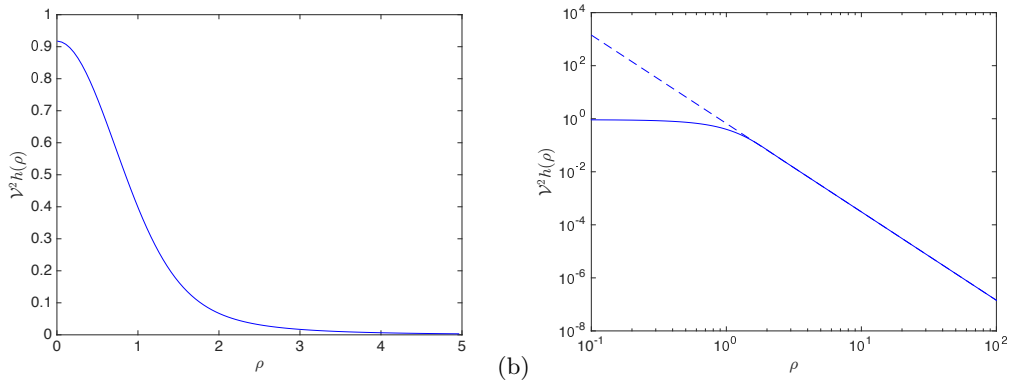

FIGURE 11. Plot of $\mathcal{V}^2h(\rho)$ (solid) given in (4.36) against ρ with (a) linear scales, (b) log–log scales. In (b) the approximation (4.37) is shown dashed.

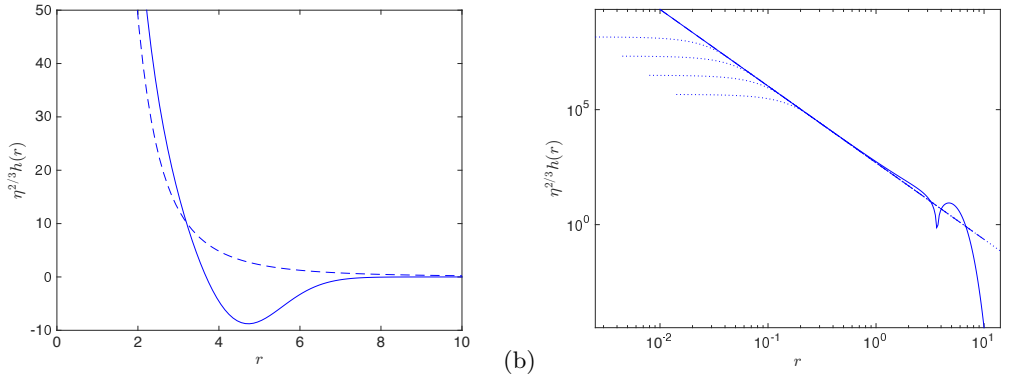

FIGURE 12. Plot of $\eta^{2/3}h(r)$ (solid) given in (4.32) for the Gaussian vortex against r with (a) linear scales, (b) log–log scales (taking the absolute value). In (a) the approximation (4.33) is shown dashed: it is also present in (b) but is somewhat overlapped with dotted curves showing $\eta^{2/3}h(\rho)$ from (4.36) plotted against r for $\eta = 10^6$ to 10^9, reading up the curves.

at a given radius r or range of radii. From the definition of $h(r)$ in (4.27) the integrated effect of the Lorentz force at radius r is sufficient to suppress the differential rotation if

$$b_0 \sim h(r)^{-1/2}. \tag{5.2}$$

Also to fix ideas we plot $h(r)$ in figure 12 for the Gaussian vortex (2.16) for a range of η values using the outer expansion (4.32) and the inner expansion (4.36).

Core formation threshold: first consider if $b_0 \gtrsim b_{\rm core}$ then at all radii r the left-hand side in (5.2) dominates. The Lorentz force (estimated by kinematic evolution) is strong enough to modify the flow field and suppress differential rotation and so flux expulsion. This represents the upper threshold for core formation. For greater fields, elastic forces dominate and prevent the onset of flux expulsion.

First of all, consider a basic estimate. The location where flux expulsion would commence is at the radius $r^\dagger$ of order unity where the differential rotation α' is maximised, and it is here or nearby where the maximum in $b_{\rm core}$ will be realised. At order one values of radius we can use (4.32) which gives $h(r) = O(\eta^{-2/3})$ and results in the threshold

$$b_{\rm core} = O(\eta^{1/3}), \tag{5.3}$$

as observed in figure 10 (upper dataset).

To improve on this, it would make sense to minimise $h(r)$ over all radii in view of (5.2) so as to maximise the field for flux expulsion to take place. However $h(r)$ has a zero crossing, and we should note that the threshold for core formation is linked to Alfvén wave generation, a process very far from the kinematic model we are using here. We do suggest instead a more precise estimate which brings in factors of α_1, taken by substituting $r^\dagger$ in (4.33) to give

$$b_{\rm core}(\eta) = c_2^{-1/2}\eta^{1/3}\alpha_1^{2/3}(r^\dagger)^{5/3}. \tag{5.4}$$

This is shown on figure 10 with good agreement, fortuitously good given that it is only correct up to a constant of unity.

Dynamical core threshold: now let us go to the other extreme. If $b_0 \lesssim b_{\rm dynam}$ then for all radii the right-hand side of (5.2) dominates and the field will remain at leading order kinematic. A core will form through flux expulsion and will shrink to an exponentially decaying remnant at the origin following BBG. We thus need to look at where the maximum of $h(r)$ is realised. From (4.33) (see also figures 11, 12), from the point of view of the outer solution, we can increase $h(r)$ by reducing r. This represents the physical fact that the flow field is 'naturally' fairly flat near the origin, the field long-lived, and the Lorentz force required to flatten it completely becomes vanishing small. However this cannot continue indefinitely and we can argue this in two ways. First of all it is clear that this increasing $h(r)$ in (4.33) (in the overlap region) must be cut off at radii $r \sim \mathcal{L} = O(\eta^{1/4})$ in (4.1) where the overlap region ends and the inner solution really takes over. Substituting this in (4.33) gives the maximum of $h(r)$ and the threshold estimated as

$$b_{\rm dynam} = O(\eta^{3/4}) \tag{5.5}$$

in agreement with figure 10 (lower dataset).

With more precision and elegance, we can move to the inner solution and figure 11(a) which shows that $\mathcal{V}^2 h$ is maximised at

$$c_4^{-2} \equiv h(0) = \int_0^\infty 3i|g|^2(f^2 - f^{*2})\,d\tau \simeq 0.91732 \tag{5.6}$$

(obtained numerically) to give

$$b_{\rm dynam} = c_4\mathcal{V} = c_4(8\eta^3 m\alpha_1)^{1/4}, \tag{5.7}$$

from (4.1). Thus we link the threshold field to the velocity scale $\mathcal{V}$ based on the inner solution, which has the crucial $\eta^{3/4}$ dependence. This is plotted in figure 10 (lower dotted line) showing good agreement up to a modest constant.

Onset of Lorentz force: finally suppose that b_0 lies in the range $b_{\rm dynam} \lesssim b_0 \lesssim b_{\rm core}$. Then flux expulsion occurs at a radius $r^\dagger$, a core is formed and a wave of flux expulsion spreads inwards. The Lorentz force however does become important at a radius $r_*(b_0)$ and time $t_*(b_0)$ given by

$$b_0 = h(r_*)^{-1/2}, \quad t_* = [\tfrac{1}{3}\eta\alpha'(r_*)^2]^{-1/3}. \tag{5.8}$$

These functions would depend on the original flow profile, but when $r_* \ll 1$ then the approximation (4.33) in the overlap region comes into play (also $\alpha'(r_*) \simeq 2\alpha_1 r_*$) and we can estimate that

$$r_* \simeq c_2^{3/10}b_0^{3/5}\eta^{-1/5}\alpha_1^{-2/5} \quad t_* \simeq c_5\eta^{-1/5}b_0^{-2/5}\alpha_1^{-2/5}, \quad c_5 = 2^{-2/3}3^{1/3}c_2^{-1/5}. \tag{5.9}$$

For example for $\eta = 10^{-7}$ and $b_0 = 10^{-5}$ we obtain $r_* \simeq 0.16$ and $t_* \simeq 2.3 \times 10^4$ in

agreement with figure 8. Note that at the lower and upper limits of the range $b_{\rm dynam} \lesssim b_0 \lesssim b_{\rm core}$, the core size is of order $\mathcal{L}$ in (4.1) and $r^\dagger$, respectively.

6. Discussion

We have studied some of the effects of dynamical feedback on flux expulsion using a quasi-linear model, using both numerical simulation and theory based on the kinematic picture. We have identified two thresholds: returning to our original dimensional formulation before (2.15) and measuring magnetic field in velocity units, the first threshold is $b_{\rm core} \sim UR_m^{-1/3}$ below which flux expulsion still operates, cutting field lines at the radius $r^\dagger$ and leaving a magnetic core within. The second is $b_{\rm dynam} \sim UR_m^{-3/4}$ below which the field evolves as in the kinematic regime. Between the two thresholds a magnetic core is formed in which the flow field near the origin is modified to be solid body rotation at leading order, so halting the diffusive decay of the core. In the range between $b_{\rm core}$ and $b_{\rm dynam}$ the core radius scales as $L(b_0/U)^{3/5}R_m^{1/5}$.†

In each case diffusive processes are key and the results depend sensitively on the magnetic diffusivity — only the cutting of fields lines by diffusion can halt the increase of Lorentz force as the field reduces in scale. With this in mind, we have made careful estimates based on the kinematic solutions, inner and outer, and we note that cruder arguments could easily lead to incorrect conclusions. For example, although the magnetic field grows linearly with time, the Lorentz force term also grows linearly in (4.23) and not quadratically as might be suggested by a simplistic estimate $\boldsymbol{b}\cdot\nabla\boldsymbol{b} \sim b^2/L$, L being the scale of the eddy, this overestimating the variation of $\boldsymbol{b}$ along field lines. Even worse would be to estimate the Lorentz force as $jb = O(t^3)$. Likewise in (4.26) it is necessary to calculate the effect of G integrated from time zero up to the time when flux expulsion occurs (similar remarks apply in the kinematic regime, as discussed in Moffatt & Kamkar (1983)). It is also important to look at the effect on the differential rotation, not the velocity or angular velocity. Finally to pick up the lower threshold $b_{\rm dynam}$ the scaling structure of the inner solution from BBG is needed, in particular relating the field magnitude to $\mathcal{V} = O(UR_m^{-3/4})$. We also note that any replacement of the true magnetic diffusion term involving the Laplacian, by some hyperdiffusion or similar cut-off would change these scaling laws. Any use of hyperdiffusion in the induction equation must be treated with caution: although the change may have a minor impact on small-scale fields at any moment, here it would have a significant impact on the large-scale, long-time evolution.

Future directions of research could include generalising the geometry, for example to an axisymmetric eddy localised in three dimensions, and a magnetic field with initially an arbitrary orientation with respect to the eddy. It would also be interesting to study other regimes of the Reynolds numbers. We have taken only $R_e \gg R_m \gg 1$, although we expect our results to have wider applicability, we think at least up to $R_e \sim R_m$. The ordering $R_e \gg R_m \gg 1$ is relevant in typical astrophysical and geophysical contexts, and so the modelling could be broadly relevant to the formation of magnetic fields in the early life of some astrophysical objects, for example the relict magnetic field likely to lie in the radiative zone of the Sun (e.g. Mestel & Weiss 1986). At least it indicates the importance of taking into account small scale reconnection processes that depend on molecular transport coefficients, even in the formation of large-scale fields, this also

† Recall that L is the spatial scale of the flow and U the velocity scale of the flow. However the actual key parameters at the lower threshold are the scale L of the flow and the magnitude of α_1 in dimensional units of (length$^2\times$ time)$^{-1}$; in other words it is appropriate to take $U = L^3\alpha_1$.

being the point originally stressed by Vainshtein & Cattaneo (1992) in the context of dynamo theory.

A related problem would be to consider an initial two-dimensional turbulent flow containing eddies or vortices, on a range of length scales: which of these would develop dynamical magnetic cores, and what would be their distribution? For what field threshold would the evolution over all length scales be entirely kinematic? Finally, it would be valuable to study dynamical flux expulsion numerically by means of full simulations in unbounded geometry and explore the limitations of the quasi-linear approximation as set out here. Simulations with $R_e \gg R_m \gg 1$ can be undertaken efficiently using contour–spectral methods (Dritschel & Tobias 2012) while regimes with $R_e \sim R_m \gg 1$ would be best simulated with standard pseudo-spectral codes.

Acknowledgements

This paper is dedicated to Konrad Bajer (Warsaw University), an inspiring colleague who contributed greatly to the field of fluid mechanics and who sadly passed away in August 2014. We thank Keith Moffatt, Andrew Soward and Nigel Weiss for useful discussions and the referees for helpful comments leading to improvements in the manuscript.

REFERENCES

Bajer, K.1998 Flux expulsion by a point vortex. *Eur. J. Mech. B/Fluids* **17**, 653–664.

Bajer, K., Bassom, A.P. & Gilbert, A.D. 2001 Accelerated diffusion in the centre of a vortex. *J. Fluid Mech.* **437**, 395–411. Referred to as BBG in the text.

Bassom, A.P. & Gilbert, A.D. 1997 Nonlinear equilibration of a dynamo in a smooth helical flow. *J. Fluid Mech.* **343**, 375–406.

Bernoff, A.J. & Lingevitch, J.F. 1994 Rapid relaxation of an axisymmetric vortex. *Phys. Fluids* **6**, 3717–3723.

Cattaneo, F. & Vainshtein, S.I. 1991 Suppression of turbulent transport by weak magnetic field. *Astrophys. J.* **376**, L21–24.

Cattaneo, F. 1994 On the effects of a weak magnetic field on turbulent transport. *Astrophys. J.* **434**, 200–205.

Dritschel, D.G. & McIntyre, M.E. 2008 Multiple jets as PV staircases: the Phillips effect and the resilience of eddy-transport barriers. *J. Atmos. Sci.* **65**, 855–874.

Dritschel, D.G. & Tobias, S.M. 2012 Two-dimensional magnetohydrodynamic turbulence in the small magnetic Prandtl number limit. *J. Fluid Mech.* **703**, 85–98.

Galloway, D.J., Proctor, M.R.E. & Weiss, N.O. 1978 Magnetic flux ropes and convection. *J. Fluid Mech.* **87**, 243–261.

Julien, K., Rubio, A.M., Grooms, I. & Knobloch, E. 2012 Statistical and physical balances in low Rossby number Rayleigh–Bénard convection. *Geophys. Astrophys. Fluid Dyn.* **106**, 392–428.

Keating, S.R. & Diamond, P.H. 2008 Turbulent resistivity in wavy two-dimensional magnetohydrodynamic turbulence. *J. Fluid Mech.* **595**, 173–202.

Keating, S.R., Silvers, L.J. & Diamond, P.H. 2008 On cross-phase and the quenching of the turbulent diffusion of magnetic fields in two dimensions. *Astrophys. J.* **678**, L137–140.

Kim, E.-J. 2006 Consistent theory of turbulent transport in two dimensional magnetohydrodynamics. *Phys. Rev. Lett.* **96**, 084504.

Mestel, L. & Weiss, N.O. 1986 Magnetic fields and non-uniform rotation in stellar radiative zones *MNRAS* **226**, 123–135.

Moffatt, H. K., 1978 *Magnetic field generation in electrically conducting fluids.* Cambridge University Press.

Moffatt, H.K. & Kamkar, H. 1983 The time-scale associated with flux expulsion. In *Stellar and planetary magnetism* (ed. A.M. Soward). Gordon and Breach.

Olver, F.J.W., Lozier, D.W., Boisvert, R.F. & Clark, C.W. 2010 *NIST handbook of mathematical functions.* Cambridge University Press.

Parker, R.L. 1966 Reconnection of lines of force in rotating spheres and cylinders. *Proc. R. Soc. Lond. A* **291**, 60–72.

Rhines, P.B. & Young, W.R. 1983 How rapidly is a passive scalar mixed within closed streamlines? *J. Fluid Mech.* **133**, 13–145.

Srinivasan, K. & Young, W.R. 2012 Zonostrophic instability. *J. Atmos. Sci.* **69**, 1633–1656.

Taylor, J.B. 1963 The magnetohydrodynamics of a rotating fluid and the Earth's dynamo problem. *Proc. R. Soc. A* **9**, 274–283.

Tobias, S.M. & Cattaneo, F. 2008 Limited role of spectra in dynamo theory: coherent versus random dynamos *Phys. Rev. Lett.* **101**, 125003

Tobias, S.M., Dagon, K.& Marston, J.B. 2011 Astrophysical fluid dynamics via direct statistical simulation. *Astrophys. J.* **727**, 127.

Vainshtein, S.I. & Cattaneo, F. 1992 Nonlinear restrictions on dynamo action *Astrophys. J.* **393**, 165–171.

Weiss, N.O. 1966 The expulsion of magnetic flux by eddies *Proc. R. Soc. Lond. A* **293**, 310–328.

Weiss, N.O. & Proctor, M.R.E. 2014 *Magnetoconvection.* Cambridge University Press.